

# Parallel solver for the three-dimensional Cartesian-grid-based time-dependent Schrödinger equation and its applications in laser- $\text{H}_2^+$ interaction studies

Y.-M. Lee,<sup>1</sup> J.-S. Wu,<sup>1,\*</sup> T.-F. Jiang,<sup>2</sup> and Y.-S. Chen<sup>3</sup>

<sup>1</sup>*Department of Mechanical Engineering, National Chiao Tung University, 1001 Ta-Hsueh Road, Hsinchu 30050, Taiwan*

<sup>2</sup>*Institute of Physics, National Chiao Tung University, 1001 Ta-Hsueh Road, Hsinchu 30050, Taiwan*

<sup>3</sup>*National Space Organization, National Applied Research Laboratories, Hsinchu 30078, Taiwan*

(Received 19 September 2007; revised manuscript received 26 October 2007; published 31 January 2008)

A parallelized three-dimensional Cartesian-grid-based time-dependent Schrödinger equation (TDSE) solver for molecules with a single electron, assuming the motion of the nucleus is frozen, is presented in this paper. An explicit stagger-time algorithm is employed for time integration of the TDSE, in which the real and imaginary parts of the wave function are defined at alternate times, while a cell-centered finite-volume method is utilized for spatial discretization of the TDSE on Cartesian grids. The TDSE solver is then parallelized using the domain decomposition method on distributed memory machines by applying a multilevel graph-partitioning technique. The solver is validated using a  $\text{H}_2^+$  molecule system, both by observing the total electron probability and total energy conservation without laser interaction, and by comparing the ionization rates with previous two-dimensional axisymmetric simulation results with an aligned incident laser pulse. The parallel efficiency of this TDSE solver is presented and discussed; the parallel efficiency can be as high as 75% using 128 processors. Finally, examples of the temporal evolution of the probability distribution of laser incidence onto a  $\text{H}_2^+$  molecule at inter-nuclear distance of 9 a.u. ( $\chi=0^\circ$  and  $90^\circ$ ) and the spectral intensities of harmonic generation at internuclear distance of 2 a.u. ( $\chi=0^\circ$ ,  $30^\circ$ ,  $60^\circ$ , and  $90^\circ$ ) are presented to demonstrate the powerful capability of the current TDSE solver. Future possible extensions of the present method are also outlined at the end of this paper.

DOI: [10.1103/PhysRevA.77.013414](https://doi.org/10.1103/PhysRevA.77.013414)

PACS number(s): 32.80.Rm, 33.80.Rv, 31.70.Hq

## I. INTRODUCTION

The hydrogen molecular ion  $\text{H}_2^+$  is the simplest molecule. It is usually used as a prototype in molecular physics, like the hydrogen atom in atomic physics. The quantum dynamics of  $\text{H}_2^+$  and other small molecules under interaction with a strong laser pulse has been a subject of continuous interest for more than two decades. Interesting phenomena such as bond softening, bond hardening, above-threshold dissociation, and Coulomb explosion have been studied [1]. In particular, a recent experiment clearly showed that the ionization rates of  $\text{H}_2^+$  at some characteristic bond lengths are greatly enhanced by a laser pulse of  $\sim 10^{14}$  W/cm<sup>2</sup> and duration of several hundreds of femtoseconds. When the molecule is ionized, the two positively charged bare ions repel each other with strong Coulomb repulsion due to the small separation between them. Suddenly the two ions fly apart rapidly [2]. This dramatic phenomenon has been named either Coulomb explosion or charge-resonance-enhanced ionization.

From the computational viewpoint, the  $\text{H}_2^+$  quantum system is not simple at all. The time evolution of  $\text{H}_2^+$  under a laser field in general has nine degrees of freedom in space plus the time variable. This kind of time-dependent Schrödinger equation (TDSE) is unlikely to be solved even using the most advanced numerical schemes and computers. The calculations are often simplified with the Born-Oppenheimer approximation (BOA) where the nuclei are

fixed during the interaction with light, because the motions of nuclei are much slower than those of electrons. It is known that the BOA is applicable when the optical period is smaller than the vibrational period.

$\text{H}_2^+$  has two fixed nuclei and a fast-moving electron. With a linearly polarized electric field along the molecular axis, the system is cylindrically symmetric in spatial coordinates in addition to the time variable. The time-dependent two-dimensional TDSE has often been used because it is computationally less demanding [e.g., [3–7]]. However, it is still very difficult (or impossible) to align the molecule to be perfectly oriented with the laser field experimentally, and also the laser field may not be linearly polarized, which makes the time-dependent three-dimensional (3D) computation of the TDSE very desirable. Unfortunately, this kind of calculation is still very limited and still in its infancy due to the very high computational cost, even with the rapid advancement of computer technology. Until very recently, there have been three types of numerical method used in solving the 3D TDSE for the study of laser-molecule interaction. (1) First the 3D TDSE was transformed from Cartesian coordinates into spheroidal coordinates and then the transformed equation was solved using the basis expansion technique with high-order Taylor's series expansion for time propagation ([8,9]; Kamta and Bandrauk [10–14]) or Legendre pseudospectral discretization (Chu and co-workers [8,15]). (2) The 3D TDSE was solved in spherical coordinates using a spherical harmonic basis expansion technique with split operator for time propagation (Madsen and co-workers [16–20]). (3) The 3D TDSE was solved directly in Cartesian coordinates using the parallel finite-difference method (FDM) [21] or finite-element method (FEM) (Collins and

\*Author to whom correspondence should be addressed. FAX: 886-3-572-0634. [chongsin@faculty.nctu.edu.tw](mailto:chongsin@faculty.nctu.edu.tw)

co-workers [21–25]; Yu and Bandrauk [26]) with split operator or high-order Taylor’s series expansion for time propagation on distributed-memory machines. The above techniques have been used successfully to study the variation of ionization rate, higher-order harmonic generation, and electron probability distribution due to changes of internuclear distance, angle of laser incidence, and laser intensity. For 3D problems, it is very time consuming to apply methods of types 1 and 2 on a single-processor machine; however, it is found difficult to parallelize the code on distributed-memory machines. In contrast, for the FDM and FEM (type 3), it is relatively easy to parallelize the simulation code. However, it is well known that with the FDM it is rather clumsy to manipulate the grid distribution. On the other hand, using the FEM often requires matrix inversion [26], if nonorthogonal-type basis functions are used, even with an explicit time-marching scheme, which is very time consuming and memory demanding in practice. If orthogonal polynomials are used as the basis functions in the FEM [21–25], then matrix inversion becomes unnecessary. Even so, the number of nonzero entries in the matrix (or memory storage) resulting from the spatial discretization and the number of machine operations per time step (or computational time) using the FEM are both large, as compared to the cell-centered finite-volume method, which will be introduced later in Sec. II. Thus, a general numerical method without the above-mentioned shortcomings, which can be used to solve the truly 3D TDSE for a general diatomic molecule (and possibly beyond) under a strong laser pulse, is still strongly desired in the physics community.

In this study, we report the development and verification of a parallelized 3D TDSE solver using a Cartesian-grid-based finite-volume method (FVM) and demonstrate its ability to simulate the physics of  $H_2^+$  under a strong laser pulse. The method we have developed here for  $H_2^+$  can readily be extended to treat general polyatomic molecules with a single active electron under a strong laser pulse.

This paper begins with a detailed description of the finite-volume method used for discretizing the 3D TDSE. The development and implementation of the parallelized TDSE solver is then outlined and simulations of a laser pulse incident along the axis of  $H_2^+$  are then carried out to verify the accuracy of the codes. These simulations are compared to the results of other studies applying the symmetric TDSE in the literature. Results for the simulated instantaneous electron probability and spectrum of harmonic generation are then presented, in which the laser is incident at different directions with respect to the  $H_2^+$  axis, to demonstrate the capability of this TDSE solver

## II. NUMERICAL METHOD

### A. Three-dimensional time-dependent Schrödinger equation

In the present study, we consider the linear time-dependent Schrödinger equation for a molecule with a single active electron under the incidence of a laser field. The TDSE can then be written as [with  $\vec{E}(\vec{r}, t)$  as the externally applied laser field],

$$i \frac{\partial \psi(\vec{r}, t)}{\partial t} = H \psi(\vec{r}, t) = \left( -\frac{1}{2} \nabla^2 + V(\vec{r}, t) \right) \psi(\vec{r}, t) \quad (1)$$

where  $\vec{r} = x\vec{i} + y\vec{j} + z\vec{k}$  is the position vector of the electron and the Hamiltonian  $H$  is expressed as the sum of the kinetic energy operator  $-\frac{1}{2}\nabla^2$  and the potential energy operator  $V(\vec{r}, t)$ . In addition, the potential energy operator under laser incidence can be generally expressed as

$$V(\vec{r}, t) = - \sum_{j=1}^N \frac{1}{|\vec{r} - \vec{R}_j|} + \vec{E}(\vec{r}, t) \cdot \vec{r}, \quad (2)$$

where  $\vec{R}_j$  and  $N$  are the position vector of nucleus  $j$  and the number of nuclei of the molecule under consideration, respectively.

### B. Discretization of the three-dimensional TDSE

As mentioned in Sec. I, very few studies have focused on direct real-space discretization of the TDSE, except those using the FDM [21] and FEM by Collins and co-workers [21–25]. It is generally agreed that for solving partial differential equations the memory storage and computational time needed using the FEM are higher than using the cell-centered FVM in achieving the same solution accuracy (see Sec. I). In the present paper, we solve the 3D TDSE directly in real-space coordinates using the cell-centered FVM, which is much simpler in practical implementation and faster in simulation speed as compared to using the FEM.

By first dividing the volume of interest into several discrete cells and applying the standard finite-volume method [27], using volume integration for the TDSE in each discrete cell, we obtain

$$i \frac{\partial}{\partial t} \int_{\Omega} \psi(\vec{r}, t) dr^3 = \int_{\Omega} \left( -\frac{1}{2} \nabla^2 + V(\vec{r}, t) \right) \psi(\vec{r}, t) dr^3, \quad (3)$$

where  $\Omega$  represents the cell volume of interest. Next, by applying the divergence theorem, Eq. (3) is reduced to

$$i \frac{\partial}{\partial t} \int_{\Omega} \psi(\vec{r}, t) dr^3 = -\frac{1}{2} \int_{\partial\Omega} \vec{\nabla} \psi(\vec{r}, t) \cdot d\vec{s} + \int_{\Omega} V(\vec{r}, t) \psi(\vec{r}, t) dr^3, \quad (4)$$

where  $\partial\Omega$  represents the cell surfaces of interest. We then apply the cell-centered finite-volume scheme, in which the wave function  $\psi$  is placed at the centroid of the cell. In the present paper, we approximate the spatial part of Eq. (4) using Cartesian-grid-based nonuniform hexahedral cells (termed a “nonconformal” mesh). A sketch of a typical mesh projected on the two-dimensional plane is shown in Fig. 1. Then, in each cell, Eq. (4) can be simply approximated as

$$i \frac{\partial}{\partial t} \psi(\vec{r}_c, t) \Delta V_{\Omega} = -\frac{1}{2} \sum_{i=1}^{N_s} [\vec{\nabla} \psi(\vec{r}_m, t) \cdot \Delta \vec{s}_i] + V(\vec{r}_c, t) \psi(\vec{r}_c, t) \Delta V_{\Omega}, \quad (5)$$

where the subscripts  $c$  and  $m$  represent the centroids of cell  $\Omega$  and surface  $\Delta s_i$ , respectively. In addition,  $N_s$  and  $\Delta V_{\Omega}$

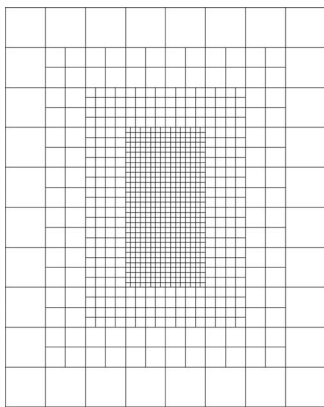


FIG. 1. Sketch of the typical finite-volume grid system projected in two-dimensional space.

represent the number of surfaces and the volume of the cell under consideration. Note that the gradient terms at the cell interface can be further approximated by a central difference scheme using the values of  $\psi$  at the centroids of neighboring cells.

The time propagation term on the left-hand side of Eq. (5) is approximated using an explicit stagger-time algorithm following the idea presented by Visscher [28] for the 1D time-dependent Schrödinger equation, in which the algorithm was shown to have second order accuracy in time for a uniform grid. The idea is described again here for completeness. The TDSE can be rewritten as

$$i \frac{\partial(R + iI)}{\partial t} = H(R + iI) \quad (6)$$

where  $\psi(\vec{r}, t) = R(\vec{r}, t) + iI(\vec{r}, t)$ , and  $R$  and  $I$  represent the real and imaginary parts of the wave function  $\psi$ , respectively. By separating these two terms, Eq. (6) can be further reduced to

$$\frac{\partial R}{\partial t} = HI, \quad (7a)$$

$$\frac{\partial I}{\partial t} = -HR. \quad (7b)$$

Then we can propagate Eqs. (7a) and (7b) alternately in time using a leapfroglike explicit scheme, termed an explicit stagger-time scheme, as follows:

$$R\left(\vec{r}, t + \frac{1}{2}\Delta t\right) = R\left(\vec{r}, t - \frac{1}{2}\Delta t\right) + \Delta t HI(\vec{r}, t), \quad t = 0 - T, \quad (8a)$$

$$I\left(\vec{r}, t + \frac{1}{2}\Delta t\right) = I\left(\vec{r}, t - \frac{1}{2}\Delta t\right) - \Delta t HR(\vec{r}, t),$$

$$t = -\frac{1}{2}\Delta t - T - \frac{1}{2}\Delta t, \quad (8b)$$

where  $T$  is the total simulation time. Data are then synchronized by simple temporal interpolation of either  $R$  or  $I$ . The initial spatial distribution of the wave function is obtained by numerically solving a previously developed eigenvalue solver for the stationary Schrödinger equation [29] using the FEM with the Jacobi-Davidson algorithm for the generalized eigenvalued matrix equation [30]. The results are then linearly interpolated on the Cartesian-grid-based nonuniform hexahedral cells, in which the values at the cell centroids are used as the initial conditions for later time propagation. In addition, absorbing-type boundary conditions [31] are employed at the outer boundaries of the computational domain, as in previous studies. Note that a larger domain size is often necessary to delay the wave reflection from the numerical boundaries, which indeed is worth studying in the future. The present TDSE solver is designed to easily set up an arbitrary number of regions having different cell sizes centered around the molecule, since most refined cells are clustered in this region (as shown in Fig. 1). In generating the nonconformal grid, we always set the ratio of cell length between two neighboring cells at the interface refined regions as 2, which further ensures numerical accuracy using this kind of mesh.

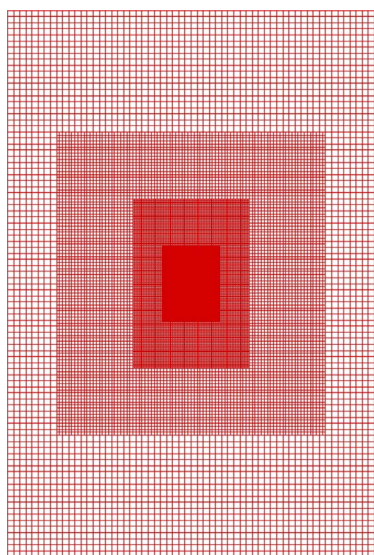
### C. Parallel implementation of TDSE solver

The above algorithm is readily parallelized through decomposition of the physical domain into groups of cells which are then distributed among the parallel processors. Each processor executes the explicit stagger-time scheme in serial for all cells in its own domain. Parallel communication between processors is required when evaluating interfacial fluxes of the wave function, requiring cell-centered data to be transferred between processors. To achieve high parallel efficiency, it is necessary to minimize the communication between processors while maintaining a balance among the computational loads on each processor. In the present study, since we have adopted a nonconformal mesh, it would be very difficult to have approximately equal numbers of cells in each processor simply by using a coordinate-based partitioning technique. Instead, we have used a publicly available multilevel graph-partitioning library [32] for decomposing the computational domain. With this library, we can easily achieve the requirement of having approximately the same number of cells in each processor with any arbitrary nonconformal mesh. Figures 2(a)–2(c), respectively, show a typical nonconformal mesh used in the present study (for 16 processors) cut through the mid-plane for solving the TDSE, domain decomposition through the mid-plane, and surface domain decomposition for the 3D mesh. Most important of all, we expect that high parallel efficiency can be obtained since we have applied the explicit stagger-time scheme for time propagation, which has minimal communication load once the load is properly balanced among processors.

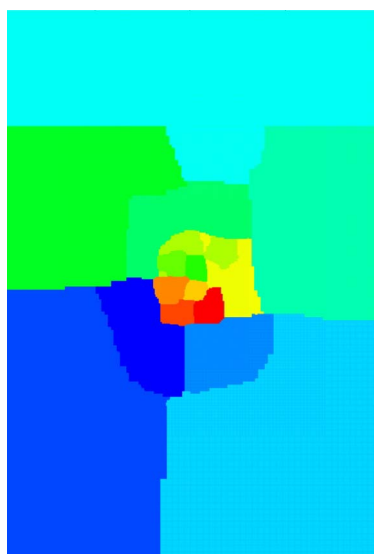
## III. CODE VERIFICATION

### A. Energy conservation of $H_2^+$ without laser incidence

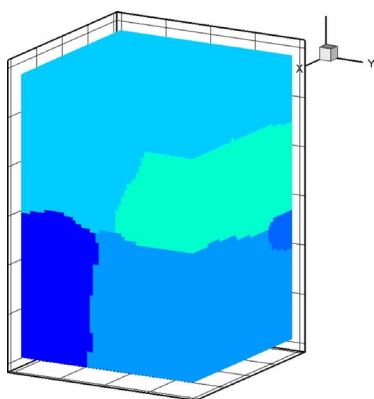
As a first verification of the implementation of the parallel TDSE solver, we have monitored the time evolution of total



(a)



(b)



(c)

FIG. 2. (Color online) (a) Typical grid system for 3D TDSE simulation (a slice through the midplane). (b) Typical slice of domain decomposition through midplane (16 processors). (c) Typical surface domain decomposition (16 processors).

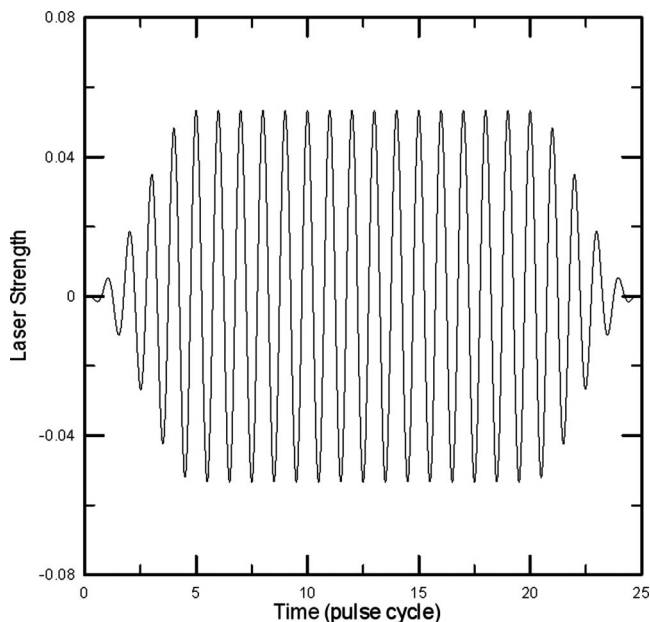


FIG. 3. Applied electric field on the  $H_2^+$  molecule along the H-H axis as a function of time. Laser intensity is  $10^{14}$  W/cm<sup>2</sup> and wavelength is 1064 nm.

energy conservation of the  $H_2^+$  molecule without laser interaction. The simulation conditions include  $2.5 \times 10^6$  hexahedral cells, 192 a.u. length in the  $x$  and  $y$  directions, 288 a.u. length in the  $z$  direction (molecular axis), a time-step size of 0.01 a.u., and internuclear distance ( $R$ ) of 9 a.u. The number

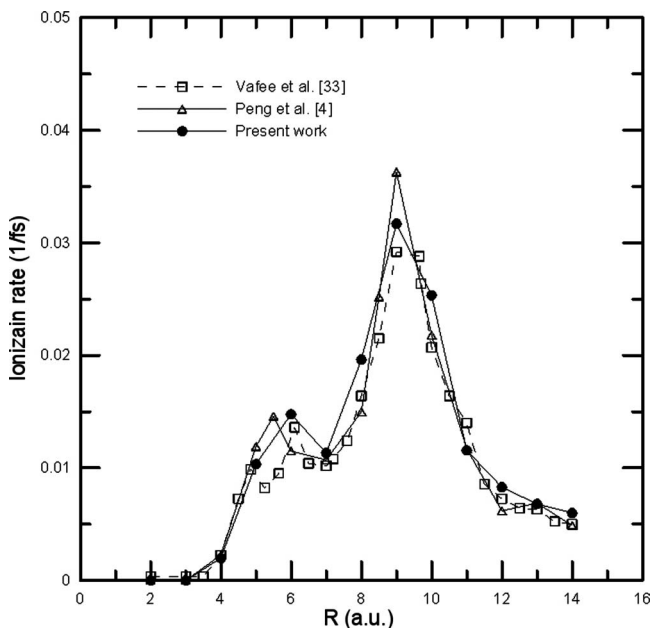


FIG. 4. Comparison of the ionization rates as a function of internuclear distance, obtained by the present parallelized 3D TDSE solver and previous 2D axisymmetric TDSE solver for an aligning subfemtosecond linearly polarized laser pulse interacting with a  $H_2^+$  molecule (power intensity is  $10^{14}$  W/cm<sup>2</sup>; wavelength is 1064 nm; and pulse duration is 25 cycles).

of processors is kept as 16, unless otherwise specified. We calculated the total energy as a function of time, and the distribution of the ground-state wave function is used as the initial condition. Results show that the total electron probability (1.0) and total energy ( $-0.6216$  eV) are both nearly conserved with very small variance of 0.001% and 0.04%, respectively, even after long-time propagation (35 fs), which demonstrates that the parallel TDSE solver is implemented correctly at least without considering an externally applied electric field.

### B. Ionization rates of $H_2^+$ with laser incidence along the H-H axis

As a further verification, we apply an intense laser pulse field to the  $H_2^+$  molecule along the direction of the H-H axis and compare the simulated ionization rates to those predicted previously using axisymmetric TDSE solvers. The applied laser pulse is the same as that in [33], as shown in Fig. 3, but related data are repeated here for completeness. The envelope of the laser pulse is  $E_0 f(t) \cos(\omega t)$ , and  $f(t)$  is defined as follows, for  $\tau_1=5$ ,  $\tau_2=15$ ,

$$f(t) = \begin{cases} \frac{1}{2} \left[ 1 - \cos\left(\frac{\pi t}{\tau_1}\right) \right], & 0 \leq t \leq \tau_1, \\ 1, & \tau_1 \leq t \leq \tau_1 + \tau_2, \\ \frac{1}{2} \left[ 1 - \cos\left(\frac{\pi t}{\tau_1}\right) \right], & \tau_1 + \tau_2 \leq t \leq 2\tau_1 + \tau_2, \\ 0 & \text{otherwise.} \end{cases} \quad (9)$$

Simulation conditions include laser intensity of  $10^{14}$  W/cm<sup>2</sup>, wavelength of 1064 nm,  $(5.5-7.5) \times 10^6$  hexahedral cells, 224–254 a.u. length in the  $z$  direction, and time-step size of 0.01 a.u.. Figure 4 illustrates a comparison of ionization rates as a function of internuclear distance among different studies. We employed Eq. (3) of Ref. [33] to calculate the ionization rate as a function of time, and then obtained the presented ionization rate by averaging over the time during which the envelope of the levels has its highest amplitude (5–20 optical cycles). Our results agree reasonably well with previous simulation data using axisymmetric TDSE codes. The well-known phenomenon, of Coulomb explosion, which has been observed experimentally, at  $R=9$  a.u. is clearly reproduced by our simulation as by other axisymmetric codes. Briefly speaking, these verifications prove that the present parallelized solver for the 3D TDSE using the finite-volume method is accurate both with and without laser incidence.

### C. Parallel performance of the 3D TDSE solver

Parallel performance of the parallel TDSE solver was tested on a PC-cluster system using Intel Itanium-2 (1.5 GHz) processors with Quadric networking at the National Center of High-Performance Computing of Taiwan. Simulation conditions are the same as those presented in Sec. III B but with  $R=9$  a.u. Figure 5 shows the parallel performance (speedup and efficiency) as a function of the proces-

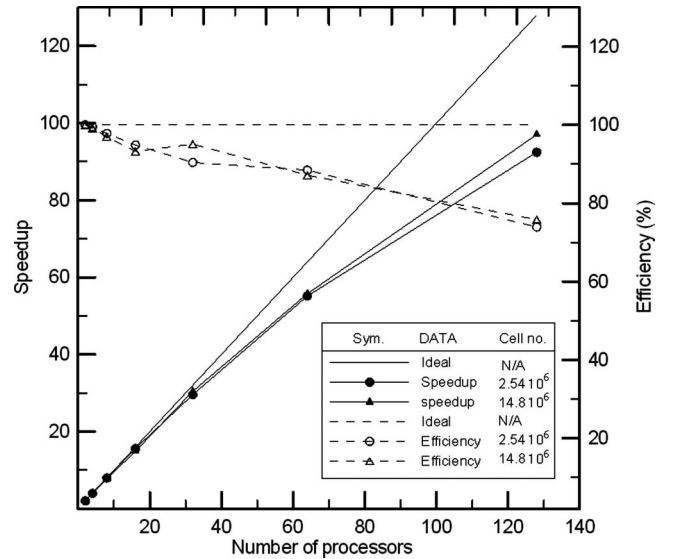


FIG. 5. Parallel efficiency of the present parallelized 3D TDSE solver as a function of the number of processors. Case 1,  $2.54 \times 10^6$  cell grid; and case 2,  $14.8 \times 10^6$  cell grid. Speedup is normalized by two-processor data.

sors for two problem sizes ( $2.54 \times 10^6$  and  $14.8 \times 10^6$  cells). The minimum number of processors used in this study is two because of memory constraints. The results show that the parallel performance efficiency, as scaled to two processors, can reach approximately 90% and 75% for 64 and 128 processors, respectively, for both problem sizes, which clearly shows that the parallel implementation is very efficient. The timing breakdown for computation and communication using various numbers of processors is summarized in Table I. Reduction of the parallel efficiency with increasing number of processors is mainly caused by the bottleneck of communication time ( $\sim 1-4$  s) regardless of the number of processors. The results show that the time for computation is much larger than that for communication between processors, which is a distinct characteristic of explicit temporal schemes, as adopted in the present study.

TABLE I. Timing breakdown of a typical parallel simulation for 400 time steps (2 545 548 cells; the time step size is 0.01 a.u.; the laser intensity is  $10^{14}$  W/cm<sup>2</sup>; and the wavelength is 1064 nm.).

Number of processors	Computation time (s)	Communication time (s)	Total time (s)	Efficiency (%)
2	528.071	1.380444	529.4514	100
4	264.4042	2.596778	267.001	99.1478
8	132.1166	4.322556	136.4391	97.0124
16	68.39622	2.587222	70.98344	93.235
32	33.80311	0.985111	34.78822	95.1205
64	17.212	1.773333	18.98533	87.1481
128	9.512111	1.399333	10.91144	75.8165

TABLE II. Simulation conditions for weaker laser incidence onto a  $\text{H}_2^+$  molecule at  $\chi=0^\circ$  and  $90^\circ$ .

	Case 1	Case 2
Angle of incidence (deg)	0	90
Laser intensity ( $10^{14}$ W/cm <sup>2</sup> )	1	1
Wavelength (nm)	1064	1064
Cell number	7 366 758	7 366 758
Simulation domain size (a.u.)	$X <  96 , Y <  96 , Z <  112 $	$X <  96 , Y <  96 , Z <  112 $
Time-step size (a.u.)	0.01	0.01
Internuclear distance (a.u.)	9	9
Pulse cycles	25 (88.589 fs)	25 (88.589 fs)

#### IV. APPLICATIONS

To demonstrate the capacity of the proposed parallel 3D TDSE solver to successfully simulate a truly 3D laser-molecule interaction, a number of simulations were conducted. They include (1) weaker laser incidence with  $\chi=0^\circ$  and  $90^\circ$  at  $R=9$  a.u., where only snapshots of electron probability are shown for comparison; (2) stronger laser incidence having different wavelengths and envelope shapes with  $\chi=0^\circ-90^\circ$  at  $R=2$  a.u., where the spectra of harmonic generations are demonstrated for comparison. In the former, the internuclear distance is intentionally chosen close to where the ionization rate is largest, as shown in Fig. 4, which makes the comparison of the electron probability distribution between  $\chi=0^\circ$  and  $90^\circ$  more distinct.

##### A. Instantaneous electron probability distribution

Important simulation conditions for a laser incident at  $\chi=0^\circ$  and  $90^\circ$ , include a laser intensity of  $10^{14}$  W/cm<sup>2</sup>, wavelength of 1064 nm, and  $R=9$  a.u. as summarized in Table II along with other simulation conditions. The computational domain consists of  $\sim 7 \times 10^6$  hexahedral cells, which are in turn divided into five regions with different sizes of cells. All domain boundaries were set with absorbing boundary conditions, as in the previous section. A time step of 0.01 a.u. was used, and  $\sim 10^5$  time steps were simulated, which required 12.5 h of simulation time using 32 processors on a PC cluster similar to that described in Sec. III C.

Figures 6 and 7 show a series of snapshots of the electron probability distribution for  $\chi=0^\circ$  and  $90^\circ$ , respectively, with internuclear distance of 9 a.u.. Figure 6 shows that, when the laser field is parallel to the molecular axis ( $\chi=0^\circ$ ), initially the electron is driven to oscillate almost in phase with the laser field and mostly in the  $z$  direction, as shown in Figs. 6(c) and 6(d), and is eventually ionized with high probability from the nucleus in the  $z$  direction. For example, near the end of the laser pulse ( $t=24.57$  optical cycles), as shown in Fig. 6(f), the electron probability near the nuclei is much smaller than that initially ( $t=0$ ), and the total electron probability is greatly reduced to 0.245, when ionization occurs. Similarly, Fig. 7 shows that when the laser field is perpendicular to the molecular axis ( $\chi=90^\circ$ ), initially the electron is driven to oscillate almost in phase with the laser field in the  $y$  direction, as shown in Figs. 7(c) and 7(d), and is eventually ion-

ized with very low probability in the  $y$  direction [Figs. 7(a) and 7(f) are almost indistinguishable]. For example, near the end of the laser pulse ( $t=24.57$  optical cycles), as shown in Fig. 7(f), the total electron probability is still as high as 0.858. By comparing the above two cases, we can conclude that it is much easier to ionize the  $\text{H}_2^+$  molecule if the laser field is aligned with the molecular axis than if the laser field is incident in other directions. This is understandable from the viewpoint of classical physics, since the Coulomb force acting on the electron due to the two nuclei is lower when the laser is parallel than when it is perpendicular to the molecular axis, if the electron is at the same distance from the molecular center.

##### B. Spectra of harmonic generations

Figure 8 shows the harmonic spectra of electron probability as a function of harmonic order (up to 50) at various angles of laser incidence with respect to the molecular axis. Note the harmonic spectrum  $S(\omega) \propto |A_{\vec{e}}(\omega)|^2$ , where  $A_{\vec{e}}(\omega)$  is defined as in Eq. (3) in [10]. Important simulation conditions include laser intensity of  $5 \times 10^{14}$  W/cm<sup>2</sup>, wavelength of 800 nm,  $R=2$  a.u., and various angles of incidence of  $\chi=0^\circ-90^\circ$ , as in [10], and are summarized in Table III along with other simulation conditions. The laser pulse is the same as employed in Ref. [10], in which there are ten pulse cycles with a sinusoidal-like envelope. Results show that the spectral intensity at some specific harmonic order generally decreases with increasing angle of laser incidence with respect to the molecular axis. In addition, the intensity decreases with increasing harmonic order for a fixed angle of incidence. Importantly, distinct peaks appear at the third, fifth, seventh, and ninth harmonic orders for angles of incidence generally showing a similar trend to those predicted by Kamata and Bandrauk [10]. However, the spectral peaks become smeared out at  $\chi=90^\circ$  because of the much smaller ionization rate at this angle.

#### V. CONCLUSIONS

In the present study, a parallel solver for the Cartesian-grid-based 3D TDSE with multiple nuclei and a single active electron using the finite-volume method was developed. The validity of the parallel solver was tested by

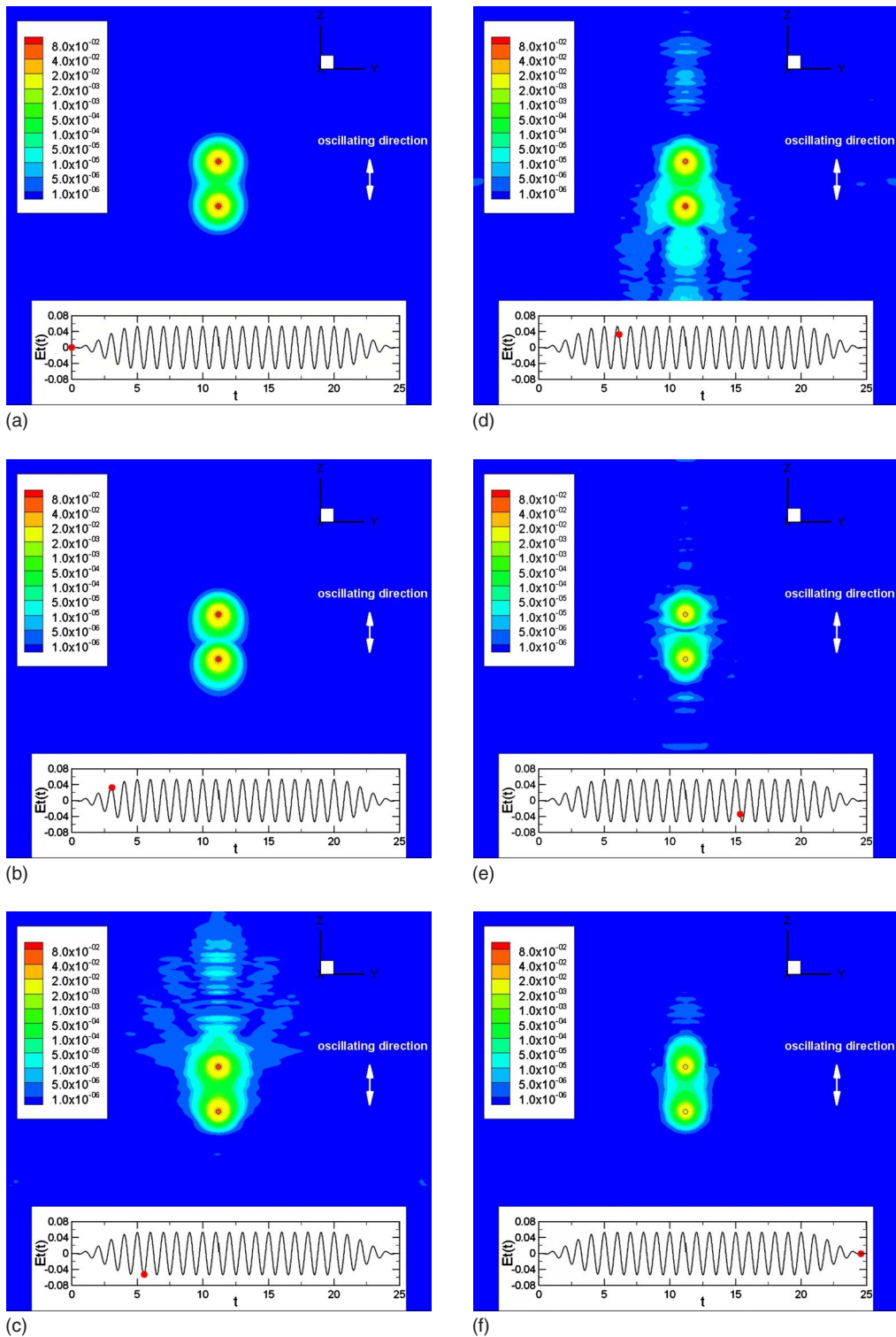


FIG. 6. (Color online) Typical snapshots of the electron probability distribution over the axisymmetric plane for a normally incident subfemtosecond linearly polarized laser pulse interacting with a  $H_2^+$  molecule ( $R=9$ ) (power intensity is  $10^{14}$  W/cm $^2$ ; wavelength is 1064 nm; pulse duration is 25 cycles; and angle of incidence is  $0^\circ$ ).

simulating the temporal conservation of electron probability and total energy of a  $H_2^+$  molecule without laser incidence, and the ionization rates of a  $H_2^+$  molecule under incidence of a laser pulse along the H-H axis. In each case, the parallel solver produced accurate results comparable to either ana-

lytical data or other simulation works using axisymmetric codes in the literature. Finally, the parallel solver was applied to simulate the response of a  $H_2^+$  molecule under laser pulse incidence at various laser field and angles of incidence to the H-H axis, which is impossible without a 3D TDSE solver.

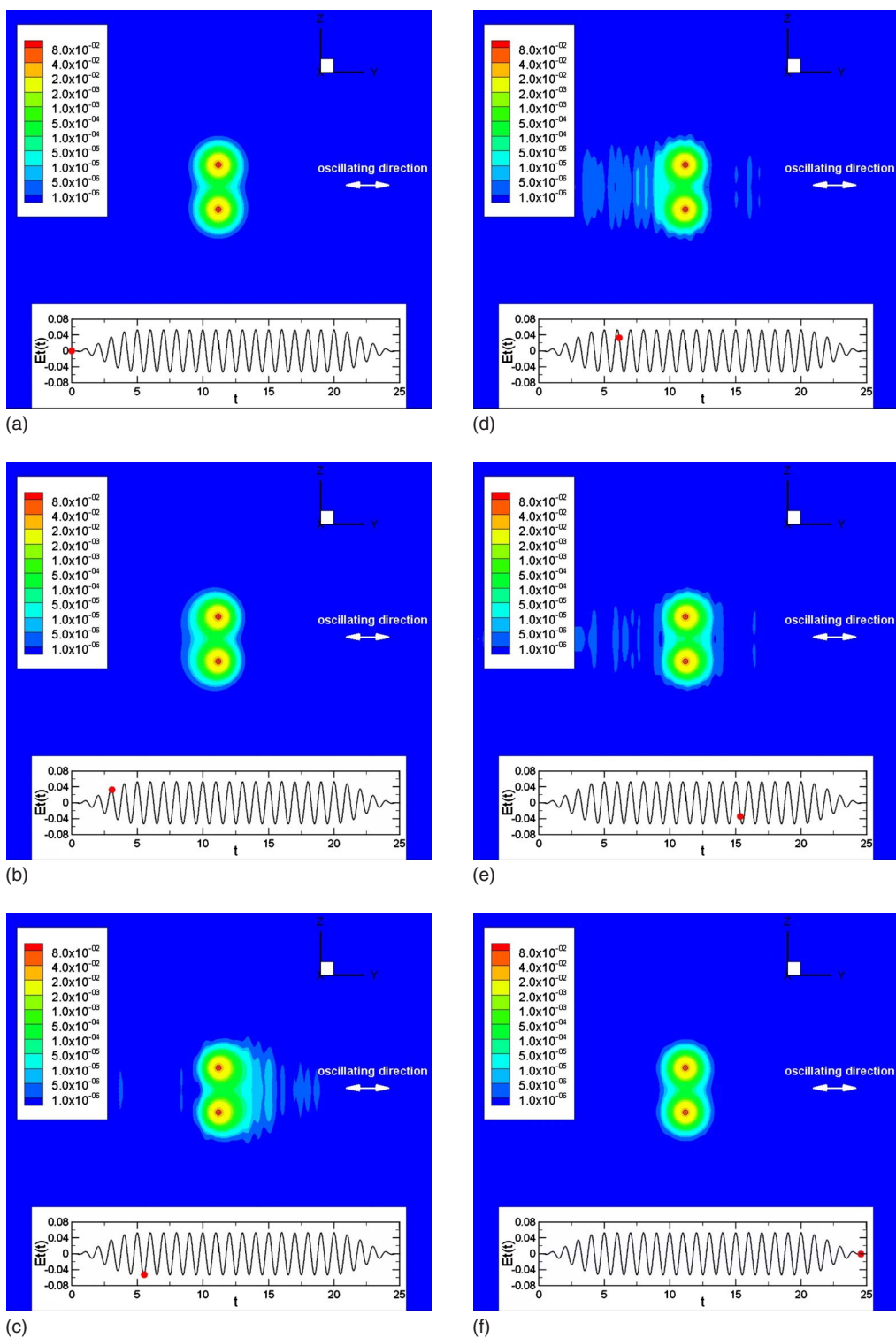


FIG. 7. (Color online) Typical snapshots of the electron probability distribution over the axisymmetric plane for a normally incident subfemtosecond linearly polarized laser pulse interacting with a  $H_2^+$  molecule ( $R=9$ ) (power intensity is  $10^{14}$  W/cm<sup>2</sup>; wavelength is 1064 nm; pulse duration is 25 cycles; and angle of incidence is  $90^\circ$ ).

The results are generally in good agreement with previous published data, wherever they are available. Several studies regarding laser-molecule interactions applying this parallel TDSE solver, which are more focused on the underlying physics, are currently in progress and will be presented else-

where in the near future. In addition, we aim to further develop the parallel 3D TDSE solver without the assumption of frozen motion of the nucleus; which allows movement of the nuclei and study of the dynamic processes during the molecule-laser interaction in a feasible way.

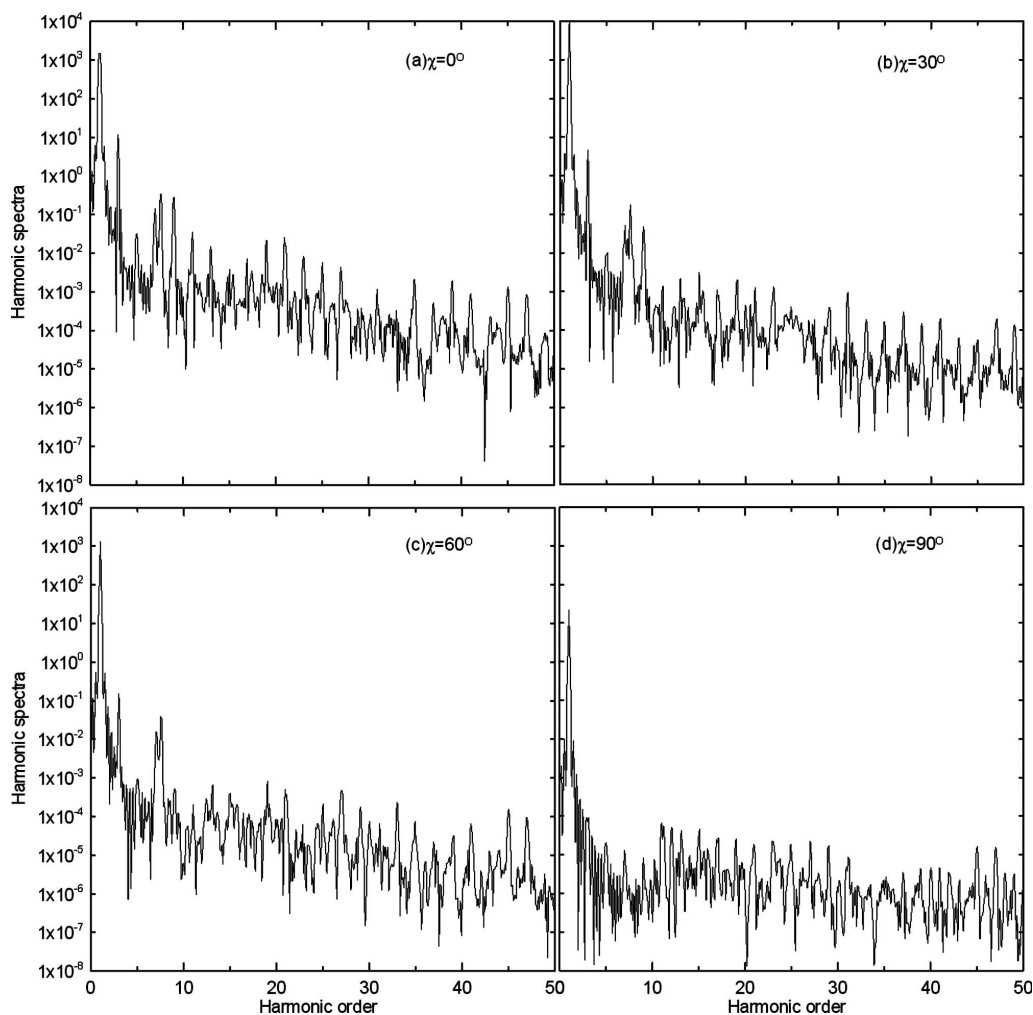


FIG. 8. Harmonic spectra of  $H_2^+$  for different orientation angles  $\chi=0-90^\circ$ . Laser intensity is  $5 \times 10^{14} \text{ W/cm}^2$  and wavelength is 800 nm. Internuclear distance is 2.0 a.u.

**ACKNOWLEDGMENTS**

This work was partially financially supported by the National Science Council of Taiwan through Grant No. NSC-

95-2221-E009-018. The parallel computing facility provided by the National Center for High-Performance Computing of Taiwan is also highly appreciated.

TABLE III. Simulation conditions for stronger laser incidence onto a  $H_2^+$  molecule at different angles of incidence ( $\chi=0^\circ, 30^\circ, 60^\circ$ , and  $90^\circ$ ).

	Case A	Case B	Case C	Case D
Oriental angle (deg)	0	30	60	90
Laser intensity ( $10^{14} \text{ W/cm}^2$ )	5	5	5	5
Wavelength (nm)	800	800	800	800
Cell number	13 461 224	13 461 224	13 461 224	13 461 224
Simulation domain size (a.u.)	$X <  112 $ $Y <  112 $ $Z <  128 $	$X <  112 $ $Y <  112 $ $Z <  128 $	$X <  112 $ $Y <  112 $ $Z <  128 $	$X <  112 $ $Y <  112 $ $Z <  128 $
Time-step size (a.u.)	0.01	0.01	0.01	0.01
Internuclear distance (a.u.)	2	2	2	2.
Pulse cycles	10 (26.6 fs)	10 (26.6 fs)	10 (26.6 fs)	10 (26.6 fs)

- [1] J. H. Posthumus, *Rep. Prog. Phys.* **67**, 623 (2004).
- [2] D. Pavičić, A. Kiess, T. W. Hänsch, and H. Figger, *Phys. Rev. Lett.* **94**, 163002 (2005).
- [3] D. Dundas, *Phys. Rev. A* **65**, 023408 (2002).
- [4] L. Y. Peng, D. Dundas, J. F. McCann, K. T. Taylor, and I. D. Williams, *J. Phys. B* **36**, L295 (2003).
- [5] M. Vafaei and H. Sabzyan, *J. Phys. B* **37**, 4143 (2004).
- [6] M. Spanner, O. Smirnova, P. B. Corkum, and M. Y. Ivanov, *J. Phys. B* **37**, L243 (2004).
- [7] M. V. Ivanov and R. Schinke, *Phys. Rev. B* **69**, 165308 (2004).
- [8] X. Chu and Shih-I Chu, *Phys. Rev. A* **63**, 013414 (2000).
- [9] B. Pons, *Phys. Rev. A* **67**, 040702(R) (2003).
- [10] G. Lagmago Kamta and A. D. Bandrauk, *Phys. Rev. A* **70**, 011404(R) (2004).
- [11] G. L. Kamta and A. D. Bandrauk, *Phys. Rev. A* **71**, 053407 (2005).
- [12] G. L. Kamta and A. D. Bandrauk, *Phys. Rev. Lett.* **94**, 203003 (2005).
- [13] G. Lagmago Kamta and A. D. Bandrauk, *Phys. Rev. A* **74**, 033415 (2006).
- [14] G. Lagmago Kamta and A. D. Bandrauk, *Phys. Rev. A* **75**, 041401(R) (2007).
- [15] D. A. Telnov and Shih-I Chu, *Phys. Rev. A* **71**, 013408 (2005).
- [16] J. P. Hansen, T. Sorevik, and L. B. Madsen, *Phys. Rev. A* **68**, 031401(R) (2003).
- [17] M. Førre, S. Selstø, J. P. Hansen, and L. B. Madsen, *Phys. Rev. Lett.* **95**, 043601 (2005).
- [18] S. Selstø, M. Førre, J. P. Hansen, and L. B. Madsen, *Phys. Rev. Lett.* **95**, 093002 (2005).
- [19] S. Selstø, J. F. McCann, M. Førre, J. P. Hansen, and L. B. Madsen, *Phys. Rev. A* **73**, 033407 (2006).
- [20] T. K. Kjeldsen, L. B. Madsen, and J. P. Hansen, *Phys. Rev. A* **74**, 035402 (2006).
- [21] Barry I. Schneider and L. A. Collins, *J. Non-Cryst. Solids* **351**, 1551 (2005).
- [22] S. X. Hu and L. A. Collins, *Phys. Rev. Lett.* **94**, 073004 (2005).
- [23] S. X. Hu and L. A. Collins, *Phys. Rev. A* **73**, 023405 (2006).
- [24] S. X. Hu and L. A. Collins, *J. Phys. B* **73**, L185 (2006).
- [25] B. I. Schneider, L. A. Collins, and S. X. Hu, *Phys. Rev. E* **73**, 036708 (2006).
- [26] H. Yu and A. D. Bandrauk, *J. Chem. Phys.* **102**, 1257 (1995).
- [27] H. K. Versteeg and W. Malasekera, *An Introduction to Computational Fluid Dynamics: The Finite Volume Method* (Addison-Wesley/Longman, Harlow, U.K., 1995).
- [28] P. B. Visscher, *Comput. Phys.* **5**, 596 (1991).
- [29] Y. M. Lee, T. F. Jiang, and J. S. Wu, in *Proceedings of the Fourth International Conference on Quantum Engineering Science*, Tainan, Taiwan, 2006.
- [30] J. G. L. Booten, H. A. van der Vorst, P. M. Meijer, and H. J. J. te Riele, CWI Report No. NM-R9414, 1994 (unpublished).
- [31] Daniel Dundas, J. F. McCann, Jonathan S. Parker, and K. T. Taylor, *J. Phys. B* **33**, 3261 (2000).
- [32] George Karypis and Vipin Kumar, *SIAM J. Sci. Comput. (USA)* **20**, 359 (1999).
- [33] Mohsen Vafaei, Hassan Sabzyan, Zahra Vafaei, and Ali Katanforoush, *Phys. Rev. A* **74**, 043416 (2006).